A Simple Way to Improve the Diurnal Cycle in Convective Rainfall over Land in Climate Models

Ian Folkins,[1] T. Mitovski,[1] J. R. Pierce[1,2]

Corresponding author: Ian Folkins, Department of Physics and Atmospheric Science, Dalhousie University, 1459 Oxford Street, P.O. Box 15000, Halifax, N.S. B3H 4R2, Canada. (ian.folkins@dal.ca)

[1] Department of Physics and Atmospheric Science, Dalhousie University, Halifax, Nova Scotia, Canada.

[2] Department of Atmospheric Science, Colorado State University, Fort Collins, CO, USA.

Abstract.

The diurnal cycle in convective rainfall over land usually peaks in the late afternoon. In most climate models, the diurnal peak in convective rainfall occurs several hours too early, and is often near local solar noon. We argue that this bias originates from the methods used in convective parameterizations to calculate the cloud base mass flux. In most convective parameterizations, the initial convective mass flux is determined from the Convective Available Potential Energy (CAPE) of a thin layer near the surface. Near surface CAPE increases rapidly during the morning when there is an increase in the upward flux of heat and water vapor. However, the mass weighted CAPE of the boundary layer as a whole responds much more slowly to the increase in downward solar radiation at the surface. Using a recently developed convective parameterization in version 4 of the Community Atmosphere Model (CAM4), we show that the overall accuracy in the diurnal simulation of convective precipitation increases as the number of near surface layers from which convective air parcels are permitted to originate increases from one to four.

1. Introduction

Most of the rainfall in the tropics, and in mid-latitudes during the summer months, originates from convective clouds. Convective rainfall over land exhibits a strong diurnal cycle, with a characteristic peak in the late afternoon or early evening [*Nesbitt and Zipser*, 2003]. This diurnal cycle has a wide range of impacts on climate forcings, surface energy and water budgets, regional circulation patterns, and atmospheric chemistry. For example, the diurnal cycle in convective rainfall gives rise to diurnal cycles in cloud amount [*May et al.*, 2012] and relative humidity which modify the propagation of solar and thermal radiation through the troposphere and affect the surface radiation balance. Regional scale sea breeze circulations, especially in the tropics, are usually driven by the diurnal variation in convective rainfall [*Ploshay and Lau*, 2010]. The diurnal cycle in the convective transport of chemical tracers from the boundary layer to the free troposphere will give rise to diurnal cycles in the free tropospheric mixing ratios of most chemical tracers. And for chemical tracers such as carbon dioxide which also exhibit strong diurnal cycles in the boundary layer [*de Arellano et al.*, 2004], the net convective transport of the chemical species from the boundary layer will depend on the phase relationship between the two diurnal cycles.

Unfortunately, the diurnal cycle in convective rainfall over land is poorly represented in many climate [*Dai*, 2006] and weather forecast [*Betts and Jakob*, 2002; *Clark et al.*, 2007] models. In many models, the diurnal peak in convective rainfall occurs several hours too early, and is often near local solar noon [*Dai*, 2006; *Bechtold et al.*, 2004]. This bias in the diurnal timing of convective rainfall will generate errors in the reflection of solar radiation back to space, especially by extensive upper tropospheric cirrus anvil clouds [*Taylor*, 2012], and is the dominant source of error in forecasts of tropical rainfall over land on short timescales [*Chakraborty*, 2010].

The absorption of solar energy by the land surface increases the upward flux of heat and water vapor, and increases the fraction of near surface air parcels with positive Convective Available Potential Energy (CAPE). The existence of near surface air with positive CAPE is a thermodynamic precondition for moist convection. In many convective parameterizations, the convective cloud base mass flux is directly related to the CAPE of a single model layer which is usually the model layer closest to the surface [*Grell*, 1993; *Jakob and Siebesma*, 2003; *Bechtold et al.*, 2001]. However, even when near surface CAPE is present, there are many physical mechanisms which can delay the onset of convective precipitation. For example, it is likely that deep convective plumes entrain air not only from the shallow surface layer, but from the entire boundary layer. In this case, the mass weighted CAPE of the boundary layer as a whole may be a better proxy for the convective cloud base mass flux than the CAPE of the near surface layer. We refer to the lag in the development of convective precipitation associated with the deepening of the convective layer as boundary layer resistance.

There are a variety of microphysical processes that contribute to delays in the development of convective precipitation. These include timescales associated with warm rain processes and the timescale required for convective plumes to rise sufficiently high that the ambient temperature is cold enough to initiate the activation of ice condensation nuclei.

The entrainment of subsaturated air from the background atmosphere into convective plumes can also be expected to delay the onset of convective precipitation. Entrainment is associated with condensate evaporation, cooling, and loss of buoyancy. Due to mixing, most convective plumes dissipate before producing precipitation. However, by moistening the local atmosphere, they diminish the impact of entrainment on the development of subsequent plumes. There can therefore be an additional delay in the onset of deep convection, equal to the timescale over which shallow convection increases the mid-level relative humidity to the threshold required to support deep convection [*Tompkins*, 2001a].

Convective precipitation often occurs in association with some form of mesoscale organization such as squall lines [*Tulich and Kiladis*, 2012]. In this case, the development of convective precipitation can be expected to be delayed by processes associated with the development of the precipitating stratiform anvil, the formation of evaporatively driven downdrafts, and the horizontal propagation of the cold pools and gust fronts that provide the vertical uplift neccessary to overcome convective inhibition and rapidly convert positive CAPE air near the surface into buoyant air within convective plumes.

Finally, at some locations, convection is associated with propagating convective systems that have been remotely generated by, for example, orography [*Ahijevych et al.*, 2004]. In this case, there would be an additional delay associated with the movement of the convective system from its place of origin.

Although there are numerous mechanisms which can delay the onset of convective rainfall over land, we show that the representation of the diurnal cycle in convective rainfall over land in a climate model can be substantially improved by a more accurate treatment of boundary layer resistance. Within each grid column, rather than restrict the initiation of convective updrafts to the model layer nearest the surface, we test for positive CAPE in each of the four lowest model layers. The initial convective mass flux therefore responds to the convective instability of the column as a whole, rather than to the CAPE of a relatively thin layer near the surface. This modification delays the onset of convective rainfall over land, and brings the diurnal rainfall peak in most regions into much better agreement with observations.

The method outlined here for improving the diurnal cycle in convective rainfall over land is quite simple, and should be relatively easy to implement in most climate models. However, there have been several other recent studies discussing ways in which the representation of the diurnal cycle in convective rainfall over land can be improved. Some models show improvement with increased horizontal resolution [*Sato et al.*, 2009; *Ploshay and Lau*, 2010; *Yamada et al.*, 2012], use of different convective parameterizations [*Liang et al.*, 2004], or changes in the triggering scheme [*Zhang*, 2003; *Xie et al.*, 2004].

Other climate models have demonstrated improvement in the diurnal cycle by incorporating some representation of convective organization into convective parameterizations. Organized mesoscale convective systems contribute to the nonlinear intensification of convective precipitation through the formation of cold pools which provide a dynamical mechanism for rapidly overcoming convective inhibition [*Tompkins*, 2001b; *Khairoutdinov and Randall*, 2006]. However, most climate models employ convective parameterizations that interact with the background atmosphere in a fixed manner. Convective organization can be introduced into convective parameterizations by using a variable from the local grid column, or output of the convective parameterization from the previous timestep, to modify the behaviour of the convective parameterization during the current timestep. Convective organization variables have included the height of the lifting condensation level [*Stratton and Stirling*, 2012], the existence of surface cold pools [*Rio et al.*, 2009], and column evaporation [*Mapes and Neale*, 2011]. These approaches have also had some success in delaying the onset of convective precipitation over land, and generating more realistic diurnal cycles [*Stratton and Stirling*, 2012; *Rio et al.*, 2009].

2. Datasets

There is significant geographic variability in the diurnal cycle of convective rainfall over land [*Yang and Slingo*, 2001]. Here, we use the Tropical Rainfall Measuring Mission (TRMM) 3B42 gridded rainfall dataset [*Liu et al.*, 2012] to determine the regional variability in the monthly mean diurnal cycle of convective rainfall. This dataset has a temporal resolution of 3 hours and a spatial resolution of 0.25°. We use TRMM 3B42 rain rates from 2003 to 2010 to calculate the mean diurnal cycle in rainfall within every CAM4 grid cell. For each land grid cell in which there is significant convective precipitation, we calculate the correlation coefficient between the TRMM diurnal cycle and the diurnal cycles of various CAM4 model simulations. The global average of this correlation coefficient is then used as an objective indicator of the fidelity with which the model matches the observed diurnal cycle.

It is desireable that climate model improvements in the diurnal cycle of convective precipitation not compromise the climatological rainfall patterns generated by a model. We therefore use monthly mean rainfall data on a 2.5 °by 2.5 °grid from the Monthly Precipitation Analysis (1979-Present) of the Global Precipitation Climatology Project (GPCP) [*Adler et al.*, 2003] to determine the accuracy of the climatological rainfall patterns generated by the CAM4-IF model.

3. Overview of the Convective Parameterization

The model simulations discussed in this paper are based on an implementation of a recently developed convective parameterization [*Folkins*, 2009] in version 4 of the Community Atmosphere Model (CAM4). During implementation, this parameterization was also modified to include a representation of subgridscale convective organization. One of the benefits of introducing convective organization is that it enabled the parameterization to exhibit a wider range of convective responses, and permitted the removal of parameterizations for both shallow [*Hack*, 1994] and deep [*Zhang and McFarlane*, 1995] convection from the default version of CAM4, and their replacement by a single convective parameterization.

There have been several changes to the convective parameterization since the initial publication [*Folkins*, 2009]. Most of these changes are related to the introduction of convective organization. These changes do not have a strong impact on the diurnal cycle, and are therefore discussed in the Appendix.

The convective parameterization is a mass flux scheme in which the effects of convective updrafts and downdrafts on the background atmosphere are represented by a spectrum of updraft and downdraft parcels moving vertically under the influence of buoyancy. The updraft parcels originate from the four model levels closest to the surface. These levels occur at roughly 980, 958, 918, and 856 hPa, corresponding to pressure thicknesses of 14.5, 29.3, 53.0, and 72.7 hPa respectively. At each of the four levels nearest the surface, we assume that subgridscale variability in temperature and relative humidity gives rise to a moist enthalpy spectrum. The width of this spectrum is an increasing function of the recent rainfall within the grid column. This enthalpy spectrum is then used to define a parcel spectrum within each near surface layer, with each parcel having the same mass per unit area. The CAPE of each parcel is evaluated independently. If it exceeds 20 J/kg, the parcel is given an initial upward kinetic energy of 20 J. The parcel then moves vertically under the influence of buoyancy using specified rules for precipitation formation and mass exchange with the background atmosphere. When the buoyancy of the parcel becomes negative, it fully detrains into the background atmosphere.

Updraft parcels produce two kinds of precipitation. If the temperature of an updraft parcel is higher than T_{freeze} (here T_{freeze} = 253 K), and the updraft parcel condensate loading exceeds a prescribed threshold, it produces updraft rain. This form of precipitation is assumed to remain within the cloud at all heights and does not evaporate. At temperatures colder than T_{freeze}, the updraft parcels produce updraft snow. This form of precipitation is assumed to remain within cloud until the melting level, at which point it exits cloud base, melts, and starts to evaporate and generate downdrafts.

In the model, the induced gridscale subsidence within a convecting grid column tends to produce positive geopotential height anomalies, and divergent outflow, in the upper troposphere. The upward gridscale motions required to balance this divergent outflow increase the relative humidity of the mid and upper troposphere. In this case, water vapor in excess of 90 % relative humidity with respect to ice within any grid box above the melting level is converted to stratiform snow. This stratiform snow is then added to the updraft snow and treated in an identical manner.

In convective regions, the upper part of the boundary layer also tends to becomes supersaturated. Below 750 hPa, we remove moisture in excess of 90 % relative humidity with a two hour timescale. The rain generated by this stratiform mechanism is added to the updraft rain, and treated in an identical manner.

Figure 1 gives a conceptual overview of the procedure used to generate downdrafts. The total snow, from both updraft and stratiform sources, is equally divided into three shafts. The three shafts are assigned lengths of 9 km, 20 km, and 45 km. The fraction of the grid column occupied by each shaft is calculated from the assumption that the local precipitation rate within each shaft is 100 mm/day. Each snow shaft is divided into 15 layers. A descending snow layer encounters cloud free air at the first model level having a temperature above 0 °C. As the layers sequentially descend through each model level, they melt within, and evaporate into, air parcels whose fractional area is equal to the fractional area of the parent snow shaft. The exposure time of a particular air parcel to a snow (rain) layer is determined in part from the remaining width of the layer and its prescribed fall speed. In general, the negative buoyancy of an air parcel will increase with the passage of every additional snow (rain) layer. When the negative buoyancy of an air parcel is sufficiently large to overcome the stability of the atmosphere, the downdraft parcel descends one model level. Due to interactions with multiple snow (rain) layers of a single snow shaft, an air parcel may descend multiple model levels within a timestep, and successively descend toward, and sometimes detrain at, the surface. This is more likely to occur for air parcels under the taller snow shafts, which have thicker snow (rain) layers, longer exposure times, and generate more intense cooling. The fall speed of the snow (rain) layers is parameterized in terms of temperature (as a surrogate for density), and typically decreases from 8 m/s just below the melting level to 5 m/s near the surface. No allowance is made for the slower fall speeds of snowflakes prior to melting.

The moist enthalpy (k_m), total water mixing ratio (r_t), and dry mass (m_d) of the updraft and downdraft parcels are updated as the parcels move vertically, mix, precipitate, and extract water from falling precipitation. Entrainment of updraft and downdraft parcels from the background atmosphere generates local sinks of k_m, r_t, and m_d, whereas parcel detrainment generates sources of conserved quantities. It is assumed that the convective parameterization does not change the top and bottom pressure levels of each grid box, and that the difference between the top and bottom pressure is related to the mass of a grid box via hydrostatic balance. At levels where the detrainment of mass exceeds entrainment, the grid box mass will exceed the hydrostatic mass (and conversely, where entrainment exceeds detrainment). To restore hydrostatic balance, the model moves mass vertically. For example, deep convection is typically associated with net mass detrainment at upper levels, and therefore triggers immediate downward subsidence within the grid column. Net upward vertical motion associated with the convective (sub-gridscale) movement of updraft and downdraft parcels is therefore usually associated with column heating.

The default CAM4 model, and the version of the model with the new convective parameterization (CAM4-IF), were run with a horizontal resolution of 1.9° $\times$ 2.5° (latitude $\times$ longitude), 26 vertical levels, and a timestep of 30 minutes. The model runs start on January 1, 2000 and end on December 31, 2002, using fixed climatological sea surface temperatures [*Gent et al.*, 2011]. The initial atmospheric state was a climatological state for the start date from the CAM4 model.

4. Results

Figure 2 shows the diurnal cycle in precipitation over land simulated by the CAM4 and CAM4-IF model runs, together with the observed diurnal cycle from the TRMM 3B42 gridded rainfall dataset. We selected four areas for comparison: the Southeast United States, Equatorial Brazil, Equatorial Africa, and Northern India. The boundaries of each region are shown in Figure 3. For simplicity, we chose areas that had weak orography. For each region, we also selected months in which there was enhanced rainfall. In all four regions, the precipitation of the default CAM4 model peaks near solar noon, a feature common to many climate models [*Bechtold et al.*, 2004; *Dai and Trenberth*, 2004]. The CAM4-IF model accurately simulates the timing of the late afternoon diurnal rainfall maximum in all four regions. Both models tend to overestimate the rainfall rate in the Equatorial Africa and Northern India regions.

The diurnal rainfall plots shown in Figure 2 suggest that the CAM4-IF model reproduces the diurnal variation in convective rainfall much more accurately than the default CAM4 model. However, it would be desirable to be able to identify the geographic regions where the CAM4-IF model fails to reproduce the diurnal cycle in convective rainfall, and to have an objective measure of the overall ability of the CAM4-IF model to simulate the diurnal cycle. The TRMM 3B42 rainfall rates were therefore first averaged to produce a new rainfall dataset having the same $1.9° \times 2.5°$ horizontal resolution as the CAM4 model grid. We then calculated the mean diurnal variation at each grid cell for every month, using TRMM rain rates from 2003 to 2010. The three years of rainfall data from the CAM4-IF model run were then used to calculate the average rain rate at the eight daily TRMM times. We then calculated, for each month, the correlation coefficient between the eight local TRMM and CAM4-IF diurnal rain rates. This was done only at land grid cells where both the TRMM and CAM4-IF monthly mean rain rates exceeded 2 mm/day, and at locations where the rainfall could be assumed to be convective. This was considered to be 20 °S - 20 °N, 40 °S - 20 °S during December - February, and 20 °N - 40 °N during June - August. Figure 3 shows the geographic distribution of the correlation coefficient, averaged over the months in which the above two conditions were satisfied. Grid cells shown in blue indicate regions where the shape of the local diurnal cycle in convective rainfall is accurately simulated by the CAM4-IF model. This includes most of Australia, the maritime continent, India, the Southeast United States, Central America, and parts of South America. The diurnal cycle is poorly simulated in Equatorial Africa, parts of China and South America, and the Midwestern United States.

At a given grid cell, there can be a variety of reasons why the local diurnal cycle in convective rainfall is poorly simulated by the CAM4-IF model. In general, however, the simulation of the local diurnal cycle in convective rainfall is poor when the local peak in convective rainfall does not occur in the late afternoon or early evening. In Figure 4, the local correlation coefficient between the CAM4-IF and TRMM diurnal cycles of a particular month is plotted against the time of the local peak in TRRM rainfall. We also plot the mean variation of the correlation coefficient against the local solar time of the TRMM rainfall maximum. The correlation coefficient is largest when the observed rainfall peak occurs between local solar noon and midnight. At other times, the correlation between the two diurnal cycles is near zero.

The dashed line of the upper panel of Figure 4 shows the variation in the frequency of occurrence of the local solar time of the TRMM diurnal rainfall maximum, at grid cells where the rainfall is considered to be convective. There is a peak in the occurrence of largest rainfall rates in the late afternoon. In roughly a quarter of all convective grid cells, the local peak in convective rainfall occurs between 16:00 and 17:00. The solid curve in the upper panel of Figure 4 shows the frequency of occurrence of peak rainfall in the CAM4-IF model. The overall shape is similar to the observed frequency of occurrence. However, the peak of the CAM4-IF curve occurs 1 hour earlier than the observed peak, indicating that peak rainfall in the CAM4-IF model continues to occur somewhat earlier than observed.

It should be noted that the 3 hour time resolution of the TRMM 3B42 dataset will give rise to an error in the time of the diurnal rainfall maximum at any given grid cell of about an hour. However, if these errors are randomly distributed, the error in the global mean estimate of the diurnal rainfall maximum from this error source should be less than an hour. The difference shown in Figure 4 in the timing of the most common diurnal rainfall maximum is therefore likely to be significant.

The upper panel of Figure 3 shows the geographic distribution of the local solar time of peak TRMM rainfall, for the month with highest rainfall. The peak in diurnal rainfall occurs at a nonstandard time for grid cells shown in dark blue (near midnight), and red and yellow (overnight). This occurs in the Sahel (e.g. Africa near 10 °N), the Himalayas, parts of Northern Australia, Argentina, the Andes, and the Midwestern United States. Many of these regions are mountainous or semi-arid, and correspond to regions of reduced correlation in the lower panel. In particular, the upper panel of Figure 3 shows that South America exhibits three nearly parallel diagonal lines of anomalous rainfall timing, one of which corresponds to the Andes. Each of these diagonal lines is associated with a similar line of reduced correlation in the lower figure.

Many of the regional anomalies in the diurnal timing of convective rainfall shown in the upper panel of Figure 3 have been previously discussed, and variously attributed to local changes in the genesis, propagation, or organization of convective systems. For example, the nighttime peak over the Great Plains of the United States has been attributed to the eastward propagation of mesoscale convective systems originating during the afternoon over the Rocky Mountains [*Dai et al.*, 1999; *Ahijevych et al.*, 2004]. Along the northeast coast of Brazil, the nocturnal maximum during January - April has been attributed to a convergence zone forming near the coast between the onshore northeasterly trade winds and an offshore land breeze, with squall lines form along the convergence zone often propagating inland [*Kousky*, 1980; *Cohen et al.*, 1995]. The middle line of maximum nighttime rainfall across Brazil appears similar to a feature that was previously tentatively attributed to a remote response to diurnally forced convection over the Andes [*Garreaud and Wallace*, 1997]. The region of anomalous diurnal timing in Northern Argentina and Paraguay corresponds to a preferred region for the development of mesoscale convective complexes [*Velasco and Fritsch*, 1987; *Salio et al.*, 2007]. Many of these features are presumably challenging to simulate in a climate model of this spatial resolution. Some of the features of the diurnal cycle in South American convective precipitation have been simulated by a regional scale model with 50 km resolution [*da Rocha et al.*, 2009]. Over the United States, there was a mixed improvement in the simulation of the diurnal cycle when the horizontal grid size was decreased from 2 °to 0.5 °[*Lee et al.*, 2007].

It is not possible to isolate a single reason for the improvement in the diurnal cycle of convective rainfall in going from the default CAM4 model to the CAM4-IF model. However, the majority of the improvement appears to result from a change in the mass flux closure. Prior to deep convection, the default CAM4 model first identifies the layer near the surface with the largest moist static energy. This is usually the layer closest to the surface. If the CAPE of this layer exceeds a threshold of 70 J/kg, mass is removed from the layer with a 1 hour timescale and entrained into a convective plume, which subsequently rises within the grid column. The CAM4-IF model, on the other hand, calculates the CAPE of the bottom four model layers. If the CAPE of any layer exceeds a threshold of 20 J/kg, mass from the layer is used to construct an updraft parcel spectrum as described in the Appendix. In this method, the total initial updraft parcel mass roughly scales with the CAPE of the boundary layer as a whole, rather than the CAPE of a relatively thin layer near the surface. This difference can affect the diurnal variation in convective rainfall generated by the two methods. Figure 5 shows the diurnal variation in the CAPE of the near surface layer of the CAM4-IF model, and of the average mass weighted CAPE of the lowest four model layers, both averaged over the Southeast United States region in July. The CAPE of the near surface layer sharply increases after sunrise and peaks near 11:00. The secondary peak near 20:00 is caused by an early evening local increase in water vapor mass mixing ratio. The mass weighted CAPE of the boundary layer responds much more slowly to the morning increase in solar insolation and reaches a maximum near 14:00.

To investigate the effect of changes in the mass flux closure on the diurnal cycle of convective rainfall, we ran five additional simulations of the CAM4-IF model. In the LEV1, LEV2, and LEV3 simulations, updraft parcels were entrained from the lowest one, two, and three model levels respectively. To compensate for the reduction in the number of pressure levels contributing to the updraft mass flux, the convective removal timescale t_{remove} was reduced to 2 (LEV1), 4 (LEV2), and 8 (LEV3) hours. We also wanted to investigate the degree to which the implementation of subgridscale organization was affecting the simulation of the diurnal cycle. We therefore ran two additional simulations.

In the NO-ORG simulation, all five organization variables were fixed at constant values. This includes (with the fixed value in brackets) the mass flux amplification factor AMP (3), the updraft parcel spectrum width dk_m (1500 J/kg), the buoyancy mixing scale b_{mix} (0.18 m/s^2), the maximum updraft condensate $r_{l,max}$ (1.6 g H_2O/kg dry air), and the updraft condensate to precipitation conversion efficiency f_{precip} (0.5). In a second simulation called NO-AMP, the mass flux amplification factor was fixed as given above, but the other four organization parameters varied as described in the Appendix.

For each of the five additional simulations, we calculated the local correlation coefficient between the TRMM and simulated diurnal cycles at grid cells considered to be convective, using the definition discussed previously. In Figure 6, we show the variation in the average value of the correlation coefficient between the model runs. The diurnal variation in convective rainfall was most poorly simulated by the default CAM4 model run, which exhibited an overall anticorrelation with TRMM rainfall on diurnal timescales. For the CAM4-IF model, there was a progressive improvement in the simulation of the diurnal cycle as additional near surface layers were permitted to generate convective updraft parcels. The additional of subgridscale convective organization was also associated with a modest improvement in the simulation of the diurnal cycle, with the average correlation coefficient of the CAM4-IF model run slightly higher than the coefficients of both NO-AMP and NO-ORG model runs.

New implementations of convective parameterizations in climate models are tested against a large number of metrics in addition to the diurnal cycle. These include climatological rainfall patterns, relative humidity and temperature profiles, conservation properties, computational efficiency, transport properties, and sources of rainfall variance such as hurricanes, equatorially trapped convectively coupled waves, and the Madden Julian Oscillation. It is desirable that increased agreement in one metric not be offset by decreased agreement in others. Space considerations preclude a full discussion of the performance of the CAM4-IF model. In our experience, however, allowing convective updraft parcels to originate from the lowest four model layers (as opposed to just the near surface layer) does not undermine other aspects of the CAM4-IF model. In particular, the accuracy of the climatological rainfall distribution of the CAM4-IF model is comparable to that of the default CAM4 model. For each month, for all convective grid cells, we calculated the correlation coefficient between the monthly mean rain rates of the two models and monthly mean GPCP rainfall. Figure 7 shows the seasonal variation of this correlation for the ocean and land grid cells. During Northern Hemisphere Fall, the climatological distribution of convective rainfall over the ocean is simulated more accurately by the default CAM4 model. Otherwise, the correlation coefficients of the CAM4 and CAM4-IF models are similar to each other.

5. Summary

Most of the convective parameterizations used in climate models are mass flux based parameterizations in which the effects of convective clouds on the background atmosphere are represented by updraft plumes or parcels moving upward under the influence of buoyancy. In many convective parameterizations, the updraft plume or parcel is usually entrained from the model level with the highest moist static energy, or a relatively thin surface layer [*Grell*, 1993; *Jakob and Siebesma*, 2003; *Bechtold et al.*, 2001]. However, there is no reason, other than computational expediency, to restrict the initiation of convective clouds exclusively to a single layer near the surface. Over the tropical oceans, the positive

CAPE surface layer typically extends to 880 hPa, while over Southeast United States, the positive CAPE layer typically extends to 840 hPa [*Mitovski et al.*, 2013]. In the default CAM4 model, due to the practice of restricting the initiation of convective plumes to the layer with highest moist static energy, convective plumes usually originate from a near surface layer that has a pressure thickness of about 14.5 hPa. In this case, in order to generate realistic deep convective mass fluxes, it is neccessary that the convective removal timescale from this layer be very short (1 hour).

The rapid removal of positive CAPE air from a thin surface layer generates a bias in the simulation of the diurnal cycle. Over land during the day, boundary layer turbulence gives rise to an upward flux of heat and water vapor from the earth's surface. This upward transport helps generate air parcels with positive CAPE throughout the boundary layer. However, due to the gradual increase in the height of the boundary layer during the day, the diurnal cycle in CAPE is altitude dependent, with CAPE in the upper part of the boundary layer exhibiting a more strongly lagged response to increases in solar insolation. As a result, the mass weighted CAPE of the boundary layer exhibits a peak at in the late afternoon. The timing of this peak is roughly in phase with the diurnal cycle in convective rainfall over land in most regions. Climate models should therefore be able to generate a reasonable cycle in convective rainfall over land, provided they use convective parameterizations which employ CAPE based mass flux closures which are sensitive to the convective instability of the grid column as a whole, rather than simply a thin surface layer. Here, we have shown that the CAM4-IF model exhibits a significant improvement in the simulation of the diurnal cycle in convective rainfall over land, as the number of near surface levels used to generate convective air parcels increases from one to four.

The method outlined here for generating the late afternoon peak in convective rainfall over land is quite simple, and seems to be the most natural explanation from an energetic point of view. However, there are numerous other physical mechanisms that can affect the timing of the diurnal peak in convective rainfall. In particular, there are many regions where the diurnal peak in convective rainfall occurs at night. Most of the rainfall in these regions appears to be associated with organized convective systems that are either remotely generated, or are associated with local synoptic forcings that favour nighttime development. In these regions, the correlation between the local diurnal cycle simulated by the CAM4-IF model and the observed diurnal cycle measured by TRMM is only weakly positive. Further improvement in the simulation of the diurnal cycle in convective rainfall over land by the CAM4-IF model will therefore require more realistic simulations of the types of convective organization that generate peak rainfall rates during the evening.

Appendix A: Subgridscale Convective Organization in the CAM4-IF Model

The one dimensional behaviour of the convective parameterization used in the CAM4-IF model has been described previously [*Folkins*, 2009]. However, during implementation in the CAM4 model, the parameterization was modified to include a form of subgridscale organization. Rather than being fixed at constant values, five of the model parameters depend on the precipitation rate generated by the model grid column over the past several hours. Although the introduction of convective organization results in only a modest improvement in the simulation of the diurnal cycle in convective rainfall over land, it does have a number of significant benefits. Due to convective organization, the convective parameterization generates a wider range of cloud types, and permits both the shallow [*Hack*, 1994] and deep [*Zhang and McFarlane*, 1995] convective schemes of the default CAM4 model to be replaced by a single convective parameterization. It also gives rise to more rapid and realistic growth and decay rates of convective precipitation, a continuous growth in the mean height of divergent outflow from shallow to deep during the development of high rain events, and a boundary layer cooling coincident with high rain rates that is roughly consistent with the observed cooling [*Mitovski et al.*, 2010].

A1. Boundary Layer Moist Enthalpy Spectrum

The variability in boundary layer temperature and specific humidity increase when convective precipitation is present [*Zhang and Klein*, 2010]. During deep convection, in cloud resolving simulations, the moist static energy of parcels recently heated by the surface can exceed the moist static energy of downdraft parcels by as much as 10 kJ/kg [*Khairoutdinov and Randall*, 2006]. Therefore, at each of the four model levels closest to the surface, we define a moist enthalpy spectrum whose width dk_m is an increasing function of the recent convective precipitation of the local grid column. The center of each moist enthalpy spectrum is equal to the moist enthalpy of the grid box. The enthalpy spectrum is used to define an updraft parcel spectrum, with each parcel having equal mass.

To define the width of the moist enthalpy spectrum, we first define a precipitation rate that is roughly equal to the local mean rate over the last several model timesteps.

$$R_{mean} = (1 - \frac{t_{step}}{\tau_{org}})R_{mean,prev} + \frac{t_{step}}{\tau_{org}}R_{current} \tag{A1}$$

In this expression, t_{step} is the timestep of the CAM4 model (30 minutes), τ_{org} is a timescale over which R_{mean} responds to changes in precipitation ($\tau_{org} = 2$ hours), $R_{mean,prev}$ is the previous local value of the mean precipitation rate, and $R_{current}$ is the current precipitation rate in the grid column. With this definition, R_{mean} is roughly equal to the mean precipitation rate of the local grid column over the time interval τ_{org}. It would be possible to simply set R_{mean} equal to the precipitation at the most recent timestep by using $\tau_{org} = t_{step}$. However, this tends to introduce excessive noise into the rainfall rate generated by the model. The convective organization variables therefore respond in a lagged manner to changes in local rainfall.

The width of the moist enthalpy spectrum is then defined using the following sigmoidal expression.

$$dk_m = dk_{m,min} + \frac{dk_{m,max}}{1 + e^{-R_{norm}}} \tag{A2}$$

$dk_{m,min}$ is a minimum width of the enthalpy spectrum, $dk_{m,min} + dk_{m,max}$ is the maximum width, and R_{norm} is defined in terms of R_{mean} and two additional rainfall parameters R_{half} and R_{scale}.

$$R_{norm} = \frac{R_{mean} - R_{half}}{R_{scale}} \tag{A3}$$

R_{half} is the rain rate at which the spectrum width is roughly equal to half its maximum value. R_{scale} is a parameter that determines the steepness of the sigmoidal curve. For small R_{scale}, the sigmoidal function approaches a step function. Figure 8 shows the dependence of dk_m on R_{mean} obtained by using the above three equations, and the parameter values given in Table 1.

If the convective precipitation within a grid column increases, the sigmoidal expression for dk_m will increase the value of dk_m parameter on the next timestep. This increase in boundary layer variance will increase the fraction of the boundary layer mass with positive CAPE, and contribute to a further increase in convective precipitation. The introduction of the dk_m parameter therefore contributes to a nonlinear intensification of high rain events, and an increase in the overall rainfall variance. It should also be noted that the downdraft formulation of the model is constructed to enable the direct injection of downdraft parcels with reduced moist static energy into the boundary layer. Without the introduction of a moist enthalpy spectrum, this direct injection of cold air would be a strong negative feedback on the development of high rain events in the model.

A2. Cloud Base Mass Flux

At each of the four lowest model levels, we define an initial updraft parcel mass per unit area spectrum $m_{p,i}$ (where i ranges from 1 to N) using the following expression.

$$m_{p,i} = \text{AMP}\Big(\frac{t_{step}}{t_{remove}}\Big)\Big(\frac{cape(i)}{cape_{scale}}\Big)\Big(\frac{dp}{gN}\Big). \tag{A4}$$

Here, dp refers to the difference between the top and bottom pressures of the layer, $cape(i)$ to the CAPE of parcel i within the enthalpy spectrum, $cape_{scale}$ is a parameter (1000 J/kg), t_{remove} a CAPE removal timescale (12 hours), and t_{step} refers to the CAM4 timestep (30 minutes).

Apart from defining an air parcel spectrum at each initial starting model level, the above expression is similar to the mass flux closures used in other convective parameterizations. Convection occurs in response to the presence of CAPE. However, we have introduced an additional parameter AMP which is also intended scale with the degree of convective organization in the grid column. We assume that the presence of convective precipitation on the previous timestep generates sub-gridscale mesoscale circulations which increase the cloud base mass flux. The dependence of the AMP parameter on the lagged mean rainfall rate R_{mean} is identical to that used for the moist enthalpy width dk_m, except that we use different parameters. These parameters are given in Table 1. The dependence of AMP on R_{mean} is also shown in Figure 8.

A3. Updraft Parcel Mixing

Air parcels with positive CAPE are given an initial upward kinetic energy of 20 J/kg to overcome the local convective inhibition. Air parcels mix with the background atmosphere using a buoyancy gradient formalism that is unchanged from the previous version of the model [*Folkins*, 2009]. The fractional entrainment (or detrainment) of mass associated with the movement of an updraft parcel from level $i-1$ with buoyancy $b_p(i-1)$, to level i with buoyancy $b_p(i)$ is given by

$$\sigma = \frac{b_p(i) - b_p(i-1)}{b_{mix}}. \tag{A5}$$

The rate with which an updraft parcel mixes with the background atmosphere is inversely proportional to a buoyancy scale parameter b_{mix}. This formalism ensures that updraft parcels entrain ($\sigma > 0$) when their buoyancy increases, and detrain ($\sigma < 0$) when they encounter stable layers and lose buoyancy. Air parcels fully detrain into the background atmosphere when their buoyancy becomes negative.

Model simulations suggest that larger deep convective updrafts mix less with their environment than smaller shallow cumulus [*Del Genio and Wu*, 2010]. The b_{mix} parameter is therefore specified to be an increasing function of R_{mean}, using the same formalism used to calculate the moist enthalpy spectrum width dk_m. The parameters used in the expressions for b_{mix} are given in Table 1, and its dependence on R_{mean} shown in Figure 8. As a result of the dependence of b_{mix} on rain rate, updraft parcels tend to have larger buoyancies, and detrain at higher altitudes, when rain rates are higher.

In order to determine the entrainment or detrainment of air at a particular model level, we calculate both a forward and a backward buoyancy gradient. Because the two buoyancy gradients may be of opposite sign, an air parcel may both entrain and detrain at a particular model level. Each model level will also contain an updraft parcel spectrum, with each parcel having different rates of entrainment and detrainment. Within the updraft parcel spectrum, the parcels with less buoyancy will have higher detrainment rates, and are preferentially removed from the updraft.

A4. Updraft Parcel Microphysics

We assume that each updraft parcel has a maximum liquid water loading $r_{l,max}$. This maximum condensate loading increases with the convective precipitation on the previous timestep, using the same procedure as used for dk_m, with the parameter values given in Table 1. This effect is intended to represent the ability of larger convective plumes with larger buoyancies and updraft velocities to retain more condensate. When the updraft parcel temperature is colder than a "freezing" temperature T_{freeze} equal to 253 K, we set $r_{l,max} = 0$. This represents the greater efficiency of precipitation formation when ice condensation nuclei are likely to be present.

A5. Fractional Conversion of Excess Condensate to Precipitation

Some fraction f_{precip} of the updraft condensate in excess of $r_{l,max}$ is converted to precipitation. The remainder is assumed to detrain into the background atmosphere (except when the background atmosphere at that particular height is saturated, in which case $f_{precip} = 1$). The efficiency with which updraft condensate is converted to precipitation increases with rain rate. We again use the same sigmoidal formalism as used for dk_m, with the parameters listed in Table 1.

Acknowledgments. This research was supported by a Discovery Grant from the Natural Sciences and Engineering Research Council of Canada (NSERC). The GPCP combined precipitation data were developed and computed by the NASA/Goddard Space

Flight Center's Laboratory for Atmospheres as a contribution to the GEWEX Global Precipitation Climatology Project.

References

Adler, R. F., G. J. Huffman, A. Chang, R. Ferraro, P. Xie, J. Janowiak, B. Rudolf, U. Schneider, S. Curtis, D. Bolvin, A. Gruber, J. Susskind, and P. Arkin (2003), The Version 2 Global Precipitation Climatology Project (GPCP) Monthly Precipitation Analysis (1979-Present), *J. Hydrometeor.*, *4*, 1147–1167.

Ahijevych, D.A., C. A. Davis, R. E. Carbone, and J. D. Tuttle (2004), Initiation of Precipitation Episodes Relative to Elevated Terrain, *J. Atmos. Sci.*, *61*, 2763–2769.

Bechtold, P., E. Bazile, F. Guichard, P. Mascart and E. Richard, (2001), A mass-flux convection scheme for regional and global models, *Q. J. R. Meteorol. Soc.*, *127*, 869–886.

Bechtold, P., J.-P. Chaboureau, A. Beljaars, A. K. Betts, M. Kohler, M. Miller and J.-L. Redelsperger, (2004), The simulation of the diurnal cycle of convective precipitation over land in a global model, *Q. J. R. Meteorol. Soc.*, *130*, 3119–3137.

Betts, A. K., and C. Jakob, (2002), Study of diurnal cycle of convective precipitation over Amazonia using a single column model, *J. Geophys. Res.*, *107*(D23), 4732, doi:10.1029/2002JD002264.

Clark, A. J., W. A. Gallus, and T.-C. Chen (2007), Comparison of the diurnal precipitation cycle in convection-resolving and non-convection-resolving mesoscale models, *Mon. Weath. Rev.*, *135*, 3456–3473.

Chakraborty, A. (2010), The skill of ECMWF medium-range forecasts during the year of tropical convection 2008, *Mon. Weath. Rev.*, *138*, 3787–3805.

Cohen, J. C. P., A. F. S. M. Dias, and C. A. Nobre (1995), Environmental conditions associated with Amazonian squall lines: A case study, *Mon. Weath. Rev.*, *123*, 3163–3174.

Dai, A., F. Giorgio, and K. E. Trenberth (1999), Observed and model-simulated diurnal cycles of precipitation over the contiguous United States, *J. Geophys. Res.*, *104*D6, 6377–6402.

Dai, A., and K. E. Trenberth (2004), The diurnal cycle and its depiction in the Community Climate System Model, *J. Clim.*, *17*, 930–951.

Dai, A., (2006), Precipitation characteristics in eighteen coupled climate models, *J. Clim.*, *19*, 4605–4630.

da Rocha, R. P., C. A. Morales, S. V. Cuadra, and T. Ambrizzi (2009), Precipitation diurnal cycle and summer climatology assessment over South America: An evaluation of Regional Climate Model version 3 simulations, *J. Geophys. Res.*, *114*, D10108, doi:10.1029/2008JD010212.

de Arellano, J.-V., B. Gioli, F. Miglietta, H. J. J. Jonker, H. K. Baltink,R. W. A. Hutjes, and A. A. M. Holtslag (2004), Entrainment process of carbon dioxide in the atmospheric boundary layer, *J. Geophys. Res.*, *109*, D18110, doi:10.1029/2004JD004725.

Folkins, I., (2009), A one-dimensional cloud model with trimodal convective outflow, *J. Clim.*, *22*, 6437–6455.

Garreaud, R. D., and J. M. Wallace (1997), The diurnal march of convective cloudiness over the Americas, *Mon. Weath. Rev.*, *125*, 3157–3171.

Gent, P. R., G. Danabasoglu, L. J. Donner, M. M. Holland, E. C. Hunke, S. R. Jayne, D. M. Lawrence, R. B. Neale, P. J. Rasch, M. Vertenstein, P. H. Worley, Z. -L. Yang, and M. Zhang (2011), The Community Climate System Model version 4, *J. Clim.*, *24*, 4973–4991.

Grell, G. (1993), Prognostic evaluation of assumptions used by cumulus parameterizations, *Mon. Weath. Rev.*, *121*, 764–787.

Hack, J. J., (1994), Parameterization of moist convection in the National Center for Atmospheric Research Community Climate Model (CCM2), *J. Geophys. Res.*, *99*, 5551–5568.

Jakob, C. and A. P. Siebesma (2003), A new subcloud model for mass-flux convection schemes: Influence on triggering, updraught properties and model climate, *Mon. Weath. Rev.*, *131*, 2765–2778.

Khairoutdinov, M., and D. Randall, (2006), High-resolution simulation of shallow-to-deep convection transition over land, *J. Atmos. Sci.*, *63*, 3421–3436.

Kousky, V. E. (1980), Diurnal rainfall variation in Northeast Brazil, *Mon. Weath. Rev.*, *108*, 488–498.

Lee, M.-I., S. D. Schubert, M. J. Suarez, I. M. Held, A. Kumar, T. L. Bell, J.-K. E. Schemm, N.-C. Lau, J. J. Ploshay, H.-K. Kim, and S.-H. Yoo (2007), Sensitivity to Horizontal Resolution in the AGCM Simulations of Warm Season Diurnal Cycle of Precipitation over the United States and Northern Mexico, *J. Clim.*, *20*, 1862–1881.

Liang, X.-Z., L. Li, A. Dai, and K. E. Kunkel (2004) Regional climate model simulation of summer precipitation diurnal cycle over the United States, *Geophys. Res. Lett.*, *31*, L24208, doi:10.1029/2004GL021054.

Liu, Z., D. Ostrenga, W. teng, and S. Kempler (2012), Tropical Rainfall Measuring Mission (TRMM) precipitation data and services for research and applications, *B. Am. Met. Soc.*, *93*, 1317–1325.

Mapes, B.E., and R. B. Neale (2011), Parameterizing convective organization to escape the entrainment dilemma, *J. Adv. Model. Earth Syst.*, *3*, M06004, doi:10.1029/2011MS000042.

May, P. T., C. N. Long, and A. Protat (2012), The diurnal cycle of the boundary layer, convection, clouds, and surface radiation in a coastal monsoon environment (Darwin, Australia), *J. Clim.*, *25*, 5309–5326.

Mitovski, T., I. Folkins, K. von Salzen, and M. Sigmond (2010), Temperature, relative humidity, and divergence response to high rainfall events in the tropics: Observations and models, *J. Clim.*, *23*, 3613–3625.

Mitovski, T., I. Folkins (2013), to be submitted.

Nesbitt, S. W., and E. Zipser (2003), The diurnal cycle of rainfall and convective intensity according to three years of TRMM Measurements, *J. Clim.*, *16*, 1456–1475.

Ploshay, J. J., and N. C. Lau (2010), Tropical Rainfall and Circulation during Boreal Summer with a High-Resolution GCM, *Mon. Wea. Rev.*, *138*, 3434–3453.

Rio, C., F. Hourdin, J.-Y. Grandpeix, and J.-P. Lafore (2009), Shifting the diurnal cycle of parameterized deep convection over land, *Geophys. Res. Lett.*, *36*, L07809, doi:10.1029/2008GL036779.

Salio, P., M. Nicolini, and E. J. Zipser (2007), Mesoscale convective systems over southeastern South American low-level jet, *Mon. Weath. Rev.*, *135*, 1290–1309.

Sato, T., H. Miura, M. Satoh, Y. N. Takayabu, and Y. Q. Wang (2009), Diurnal Cycle of Precipitation in the Tropics Simulated in a Global Cloud-Resolving Model, *J. Clim.*, *22*, 4809–4826.

Stratton, R. A., and A. J. Stirling (2012), Improving the diurnal cycle of convection in GCMs, *Q. J. R. Meteorol. Soc.*, *138*, 1121–1134.

Taylor, P. C. (2012), Tropical outgoing longwave radiation and longwave cloud forcing diurnal cycles from CERES, *J. Atmos. Sci.*, *69*, 3652–3669.

Tompkins, A. M. (2001), Organization of tropical convection in low vertical wind shears: The role of water vapor, *J. Atmos. Sci.*, *58*, 529–545.

Tulich, S. N., G. N. Kiladis (2012), Squall lines and convectively coupled gravity waves in the tropics: Why do most cloud systems propagate westward? *J. Atmos. Sci.*, *16*, 2995–3012.

Tompkins, A. M. (2001), Organization of tropical convection in low vertical wind shears: The role of cold pools, *J. Atmos. Sci.*, *58*, 1650–1672.

Velasco, I., and J. M. Fritsch (1987), Mesoscale convective complexes in the Americas, *J. Geophys. Res.*, *92*, 9591–9613, doi:10.1029/ JD092iD08p09591.

Xie, S., M. Zhang, J. S. Boyle, R. T. Cederwall, G. L. Potter, and W. Lin (2004), Impact of a revised convective triggering mechanism on community atmosphere model, version 2, simulations: Results from short-range weather forecasts, *J. Geophys. Res.*, *109*, D14102, doi:10.1029/2004JD004692.

Yamada, T. J., M. Lee, M. Kanamitsu, H. Kanamaru (2012), Diurnal Characteristics of Rainfall over the Contiguous United States and Northern Mexico in the Dynamically Downscaled Reanalysis Dataset (US10), *J. Hydrometeor.*, *13*, 1142–1148.

Yang, G.-Y. and J. Slingo (2001), The diurnal cycle in the tropics. *Mon. Weath. Rev.*, *129*, 784–801.

Zhang, G. J., and N. A. McFarlane (1995), Sensitivity of climate simulations to the parameterization of cumulus convection in the Canadian Climate Centre general circulation model, *Atmosphere-Ocean*, *33*, 407–446.

Zhang, G. J., (2003), Roles of tropospheric and boundary layer forcing in the diurnal cycle of convection in the U.S. Southern Great Plains, *Geophys. Res. Lett.*, *30*(24), 2281, doi:10.1029/2003GL018554.

Zhang, Y., and S. A. Klein (2010), Mechanisms affecting the transition from shallow to deep convection over land: Inferences from observations of the diurnal cycle collected at the ARM Southern Great Plains site, *J. Atmos. Sci.*, *67*, 2943–2959.

Variable	R_{scale}	R_{half}	Min Value	Max value	Description
AMP	15 mm/day	45 mm/day	1	25	parcel mass amplification factor
dk_m	15 mm/day	35 mm/day	500 J/kg	6000 J/kg	parcel enthalpy spectrum width
b_{mix}	15 mm/day	40 mm/day	0.12 m/s^2	0.18 m/s^2	mixing buoyancy scale
$r_{l,max}$	15 mm/day	40 mm/day	1 g/kg	3 g/kg	updraft condensate maximum
f_{precip}	10 mm/day	15 mm/day	0.3	0.7	condensate precipitation fraction

Table 1. Parameter values for the variables which are assumed to depend on the local degree of convective organization. For each variable, the four parameters listed here are used to calculate a sigmoidal value of the variable using Eqs. (1) and (2).

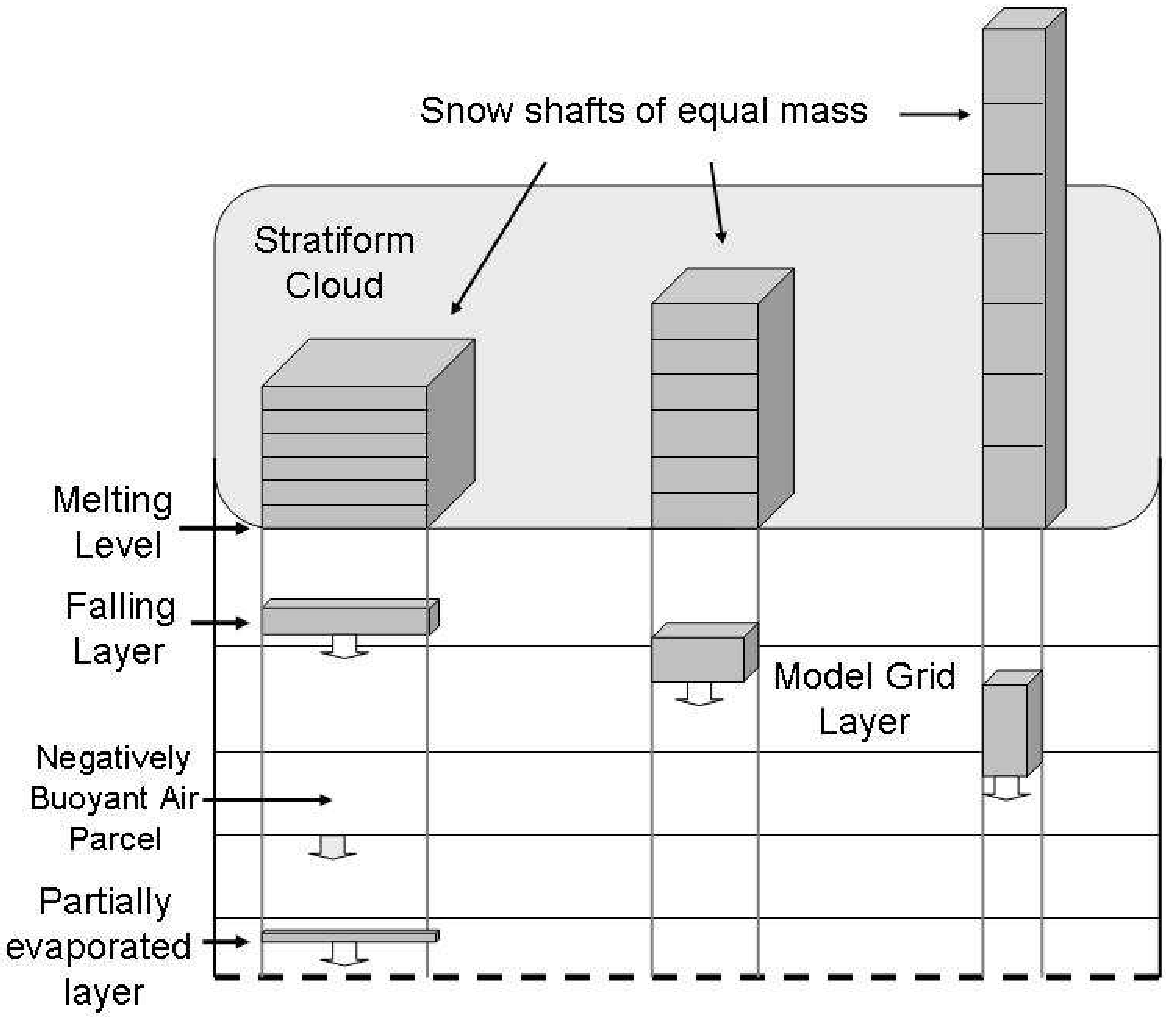

Figure 1. A conceptual diagram of the downdraft formalism of the convective parameterization. See the text for explanation.

Gri-2.12.23 /misc/users/clouds/folkins/BUBBLE/diurn/areas.gri (Wed May 8 11:28:24 2013)

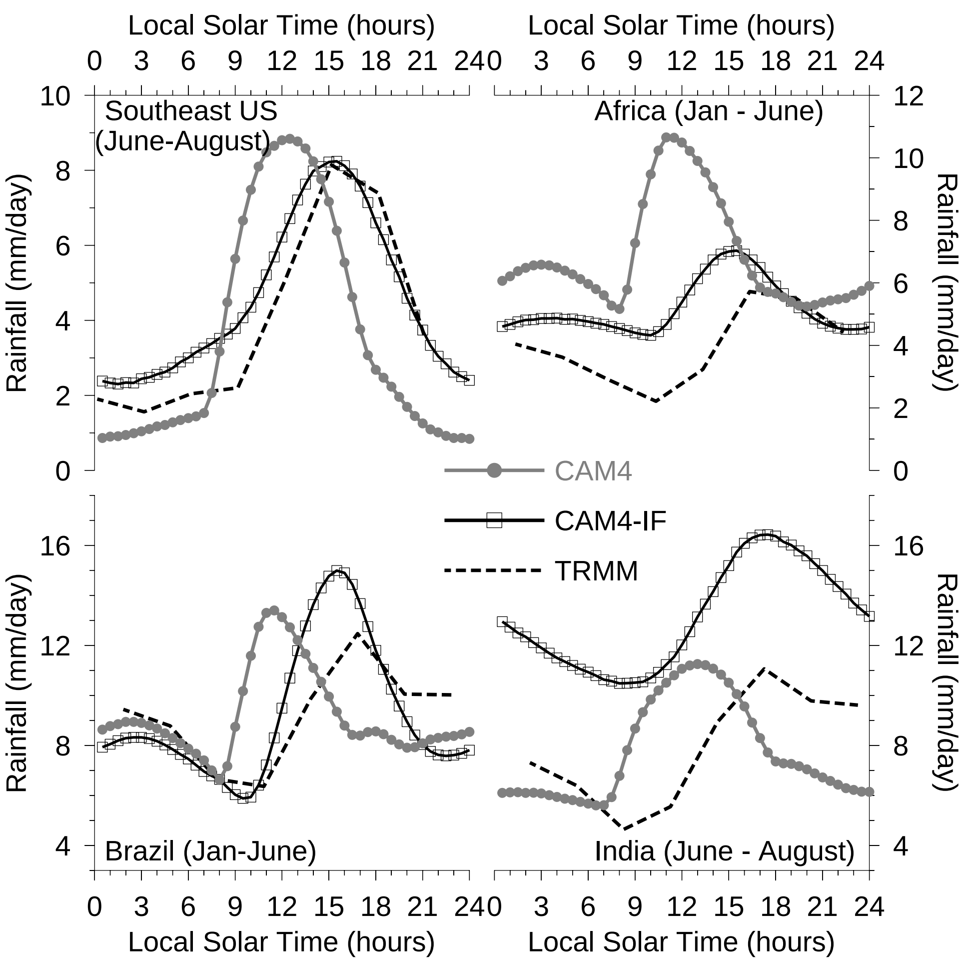

Figure 2. Each curve refers to the diurnal variation in rainfall of one of the four regions shown in Figure 3. Dashed curve: TRMM 3B42. Gray curves with solid circles: default CAM4 model. Black curves with open boxes: CAM4-IF model.

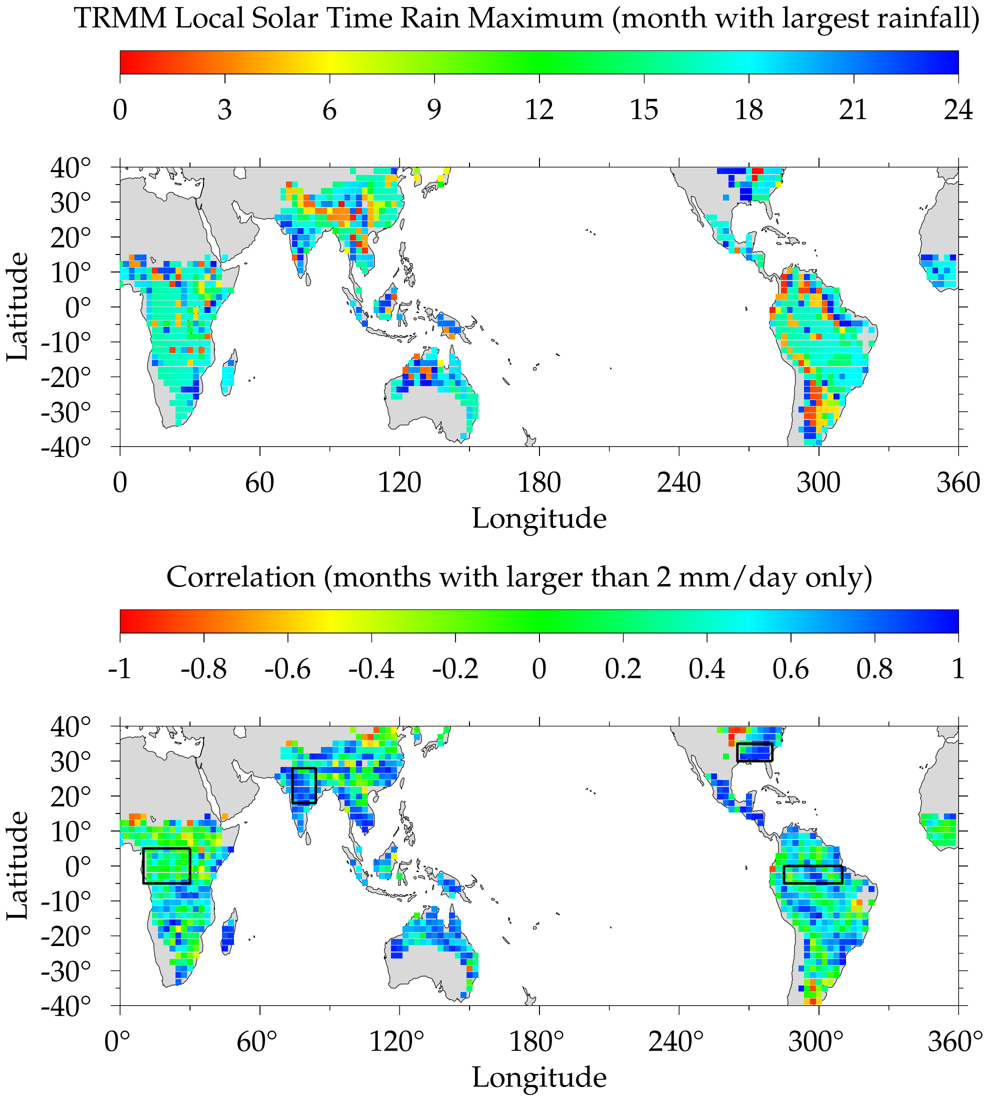

Figure 3. (upper) The local solar time of the diurnal peak in TRMM 3B42 rainfall, during the month with the largest mean rainfall. (lower) Correlation between the CAM4-IF and TRMM diurnal rainfall cycles, averaged over the months in which the mean rainfall rate of both datasets exceeds 2 mm/day.

Gri-2.12.23 /misc/users/clouds/folkins/BUBBLE/diurn/lst.gri (Wed May 8 11:28:26 2013)

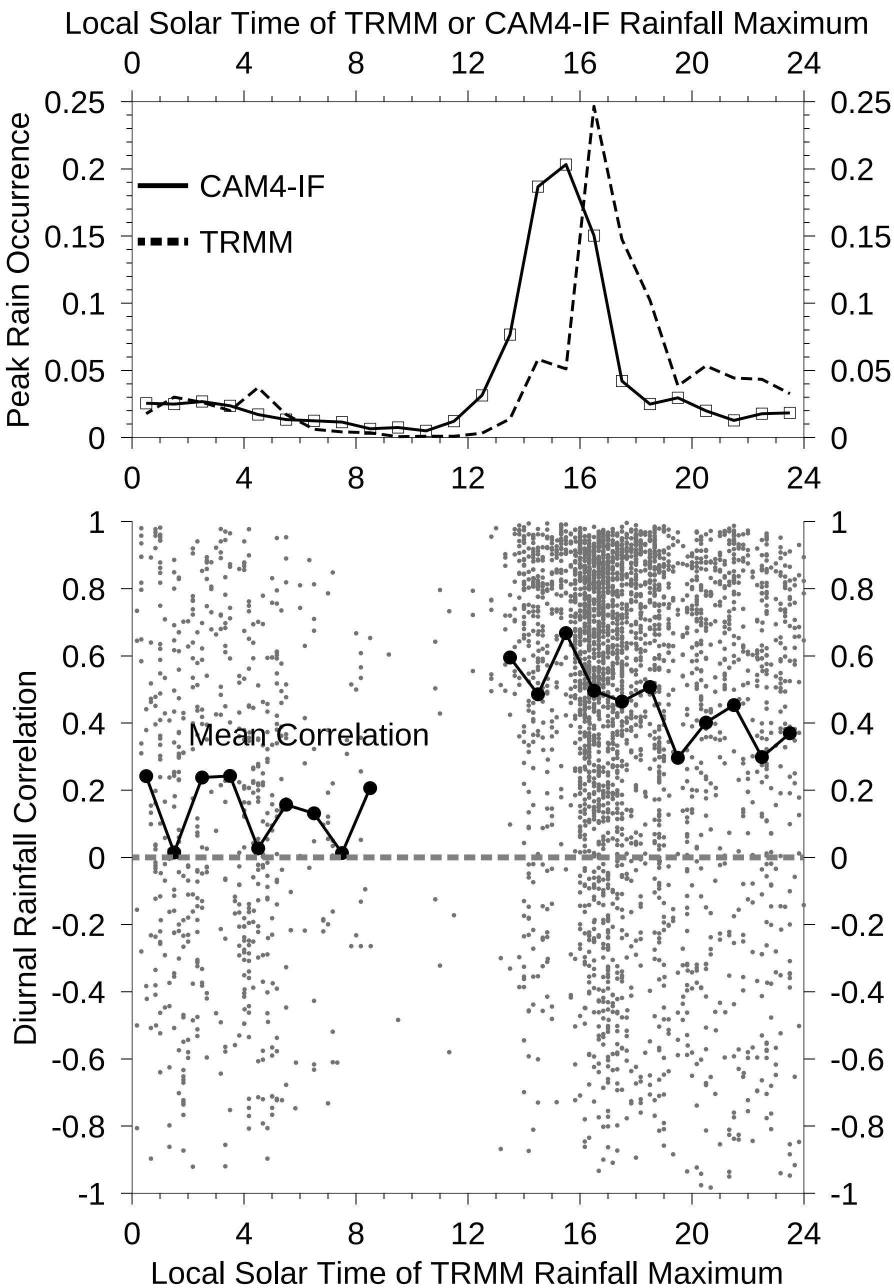

Figure 4. (upper) Dashed curve: the frequency of occurrence of the local time of peak TRMM 3B42 rainfall, for land grid cells where the monthly mean rain rate exceeds 2 mm/day. Solid curve: the frequency of occurrence of the local time of peak rainfall from the CAM4-IF model. (lower) Gray dots show the correlation between the local CAM4-IF and TRMM diurnal cycles, plotted against the local time of the TRMM rainfall peak. The solid curve was obtained by binning the correlation coefficients in increments of one hour.

Gri-2.12.23 /misc/users/clouds/folkins/BUBBLE/diurn/cape.gri (Wed May 8 11:28:27 2013)

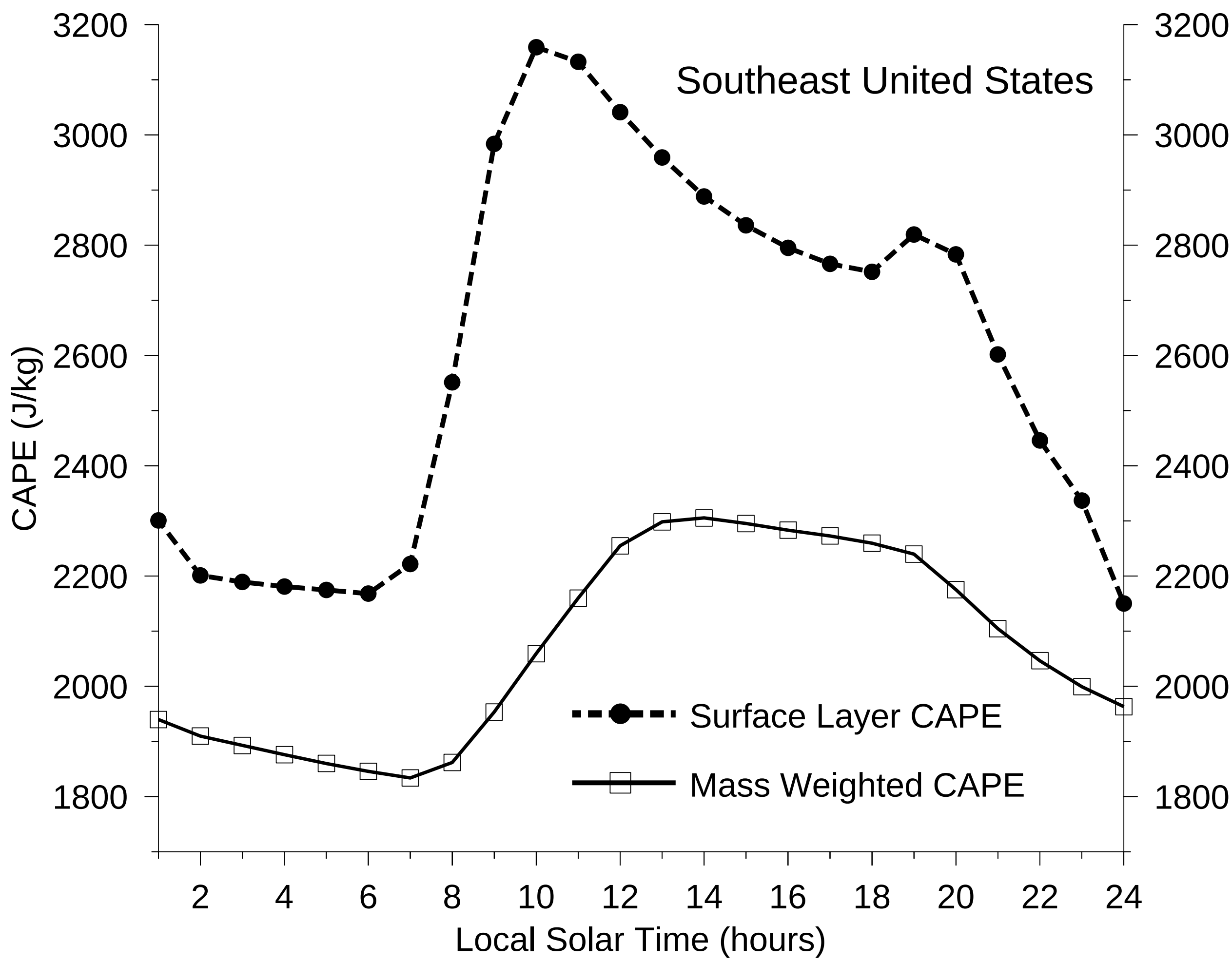

Figure 5. The diurnal variation of the CAPE of the surface layer (dashed) and the mass weighted CAPE of the lowest four model layers (solid), of the CAM4-IF model in the Southeast United States Region during July.

Gri-2.12.23 /misc/users/clouds/folkins/BUBBLE/diurn/r.mod.gri (Wed May 8 11:28:28 2013)

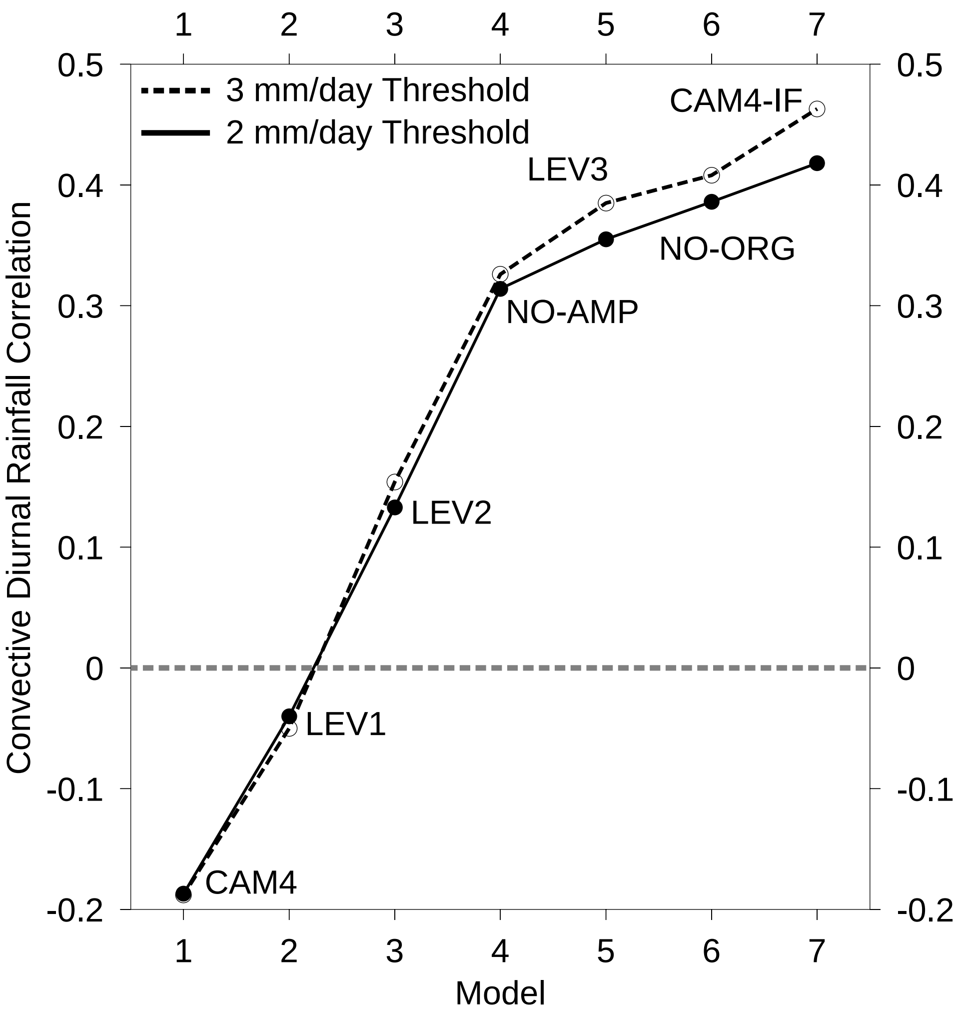

Figure 6. For each model simulation, we calculated the local correlation coefficient between the diurnal cycle in convective rainfall calculated by the model and the diurnal cycle calculated from the TRMM 3B42 dataset. A mean correlation coefficient was calculated by averaging over all land grid cells where the rainfall was likely to be convective. The solid line shows the dependence of the average correlation on the model simulation where we applied a rain threshold to each grid cell of 2 mm/day. The dashed curve used a rain threshold of 3 mm/day.

Gri-2.12.23 /misc/users/clouds/folkins/BUBBLE/diurn/r.gri (Wed May 8 11:28:29 2013)

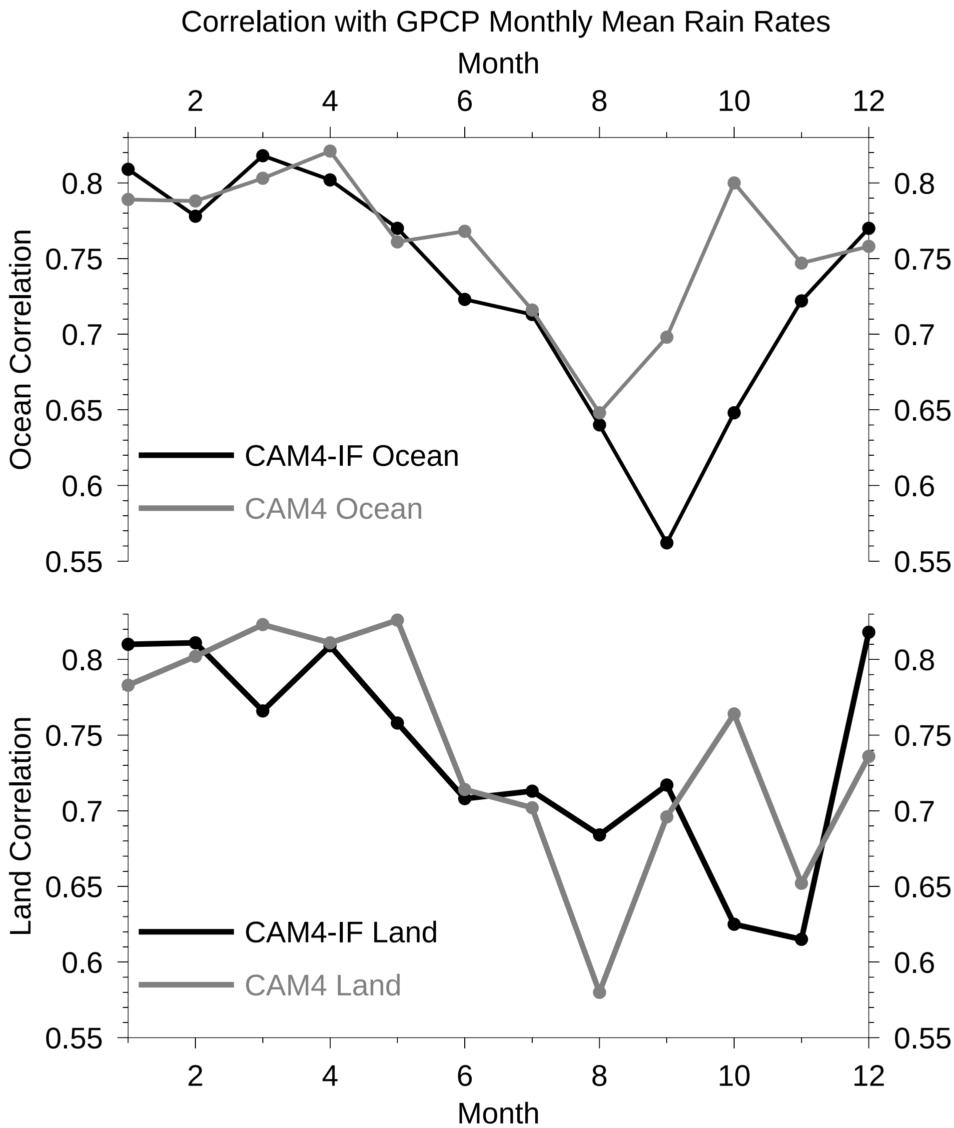

Figure 7. Three year runs of the CAM4 and CAM4-IF models were used to generate monthly mean rainfall rates. For each month, we calculated the overall correlation with monthly mean GPCP rain rates using grid cells at which the rain was likely to be convective. (upper) Seasonal variation of the correlation coefficient using ocean grid cells. (lower) Seasonal variation of the correlation coefficient using land grid cells.

Gri-2.12.23 /misc/users/clouds/folkins/BUBBLE/diurn/km.gri (Wed May 8 11:28:30 2013)

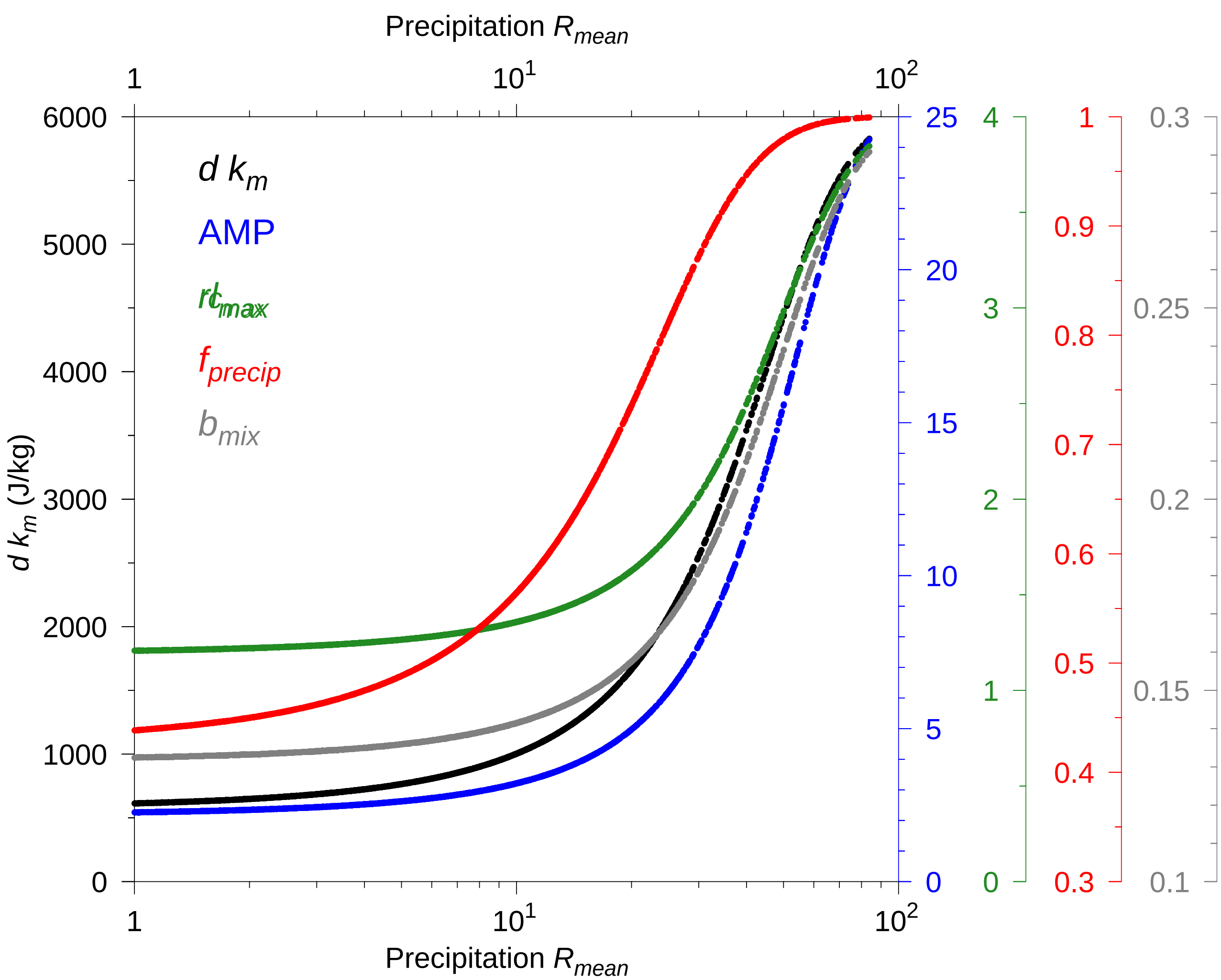

Figure 8. Each curve shows the sensitivity of a particular variable used in the convective parameterization to R_{mean}, roughly equal to the mean rainfall rate of a grid column over the previous two hours. The formulas used to calculate the sigmoidal curves are given in the Appendix. At low values of R_{mean}, the variables variable converge to the minimum value listed in Table 1. At large values of R_{mean}, the variables converge toward the sum of the minimum and maximum values listed in Table 1.